ACS OMEGA

Open Access

http://pubs.acs.org/journal/acsodf

Article

Carbon-Supported Nanocomposite Synthesis, Characterization, and Application as an Efficient Adsorbent for Ciprofloxacin and Amoxicillin

Maria Sadia, Izaz Ahmad, Shaukat Aziz, Rizwan Khan, Muhammad Zahoor,* Riaz Ullah, and Essam A. Ali

Cite This: *ACS Omega* 2024, 9, 6815−6827

Read Online

ACCESS | Metrics & More | Article Recommendations | Supporting Information

ABSTRACT: The existence of antibiotics in the environment has recently raised serious concerns about their possible hazards to human health and the water ecosystem. In the current study, an activated carbon-supported nanocomposite, AC-$CoFe_2O_3$, was synthesized by a coprecipitation method, characterized, and then applied to adsorb different drugs from water. The synthesized composites were characterized by using energy-dispersive X-ray spectroscopy, Fourier transform infrared spectroscopy, Brunauer−Emmett−Teller plots, and scanning electron microscopy. The adsorption of both Ciprofloxacin (Cipro) and Amoxicillin (Amoxi) antibiotics on the composite followed the pseudo-second-order kinetic model (R^2 = 0.9981 and 0.9974 mg g^{-1} min^{-1}, respectively). Langmuir isotherm was the best-fit model showing 312.17 and 217.76 mg g^{-1} adsorption capacities for Ciprofloxacin and Amoxicillin, respectively, at 333 K. The negative Gibbs free energy ($\Delta G°$) specified the spontaneity of the method. The positive change in the enthalpy (ΔH) indicated that the adsorption process was assisted by higher temperatures. The different optimized parameters were pH, contact time, adsorbent weight, concentration, and temperature. The maximum adsorption of Cipro was found to be 98.41% at pH 12, while for Amoxi, it was 89.09% at pH 2 at 333 K. The drugs were then successfully determined from natural water samples at optimized conditions using these nanocomposites.

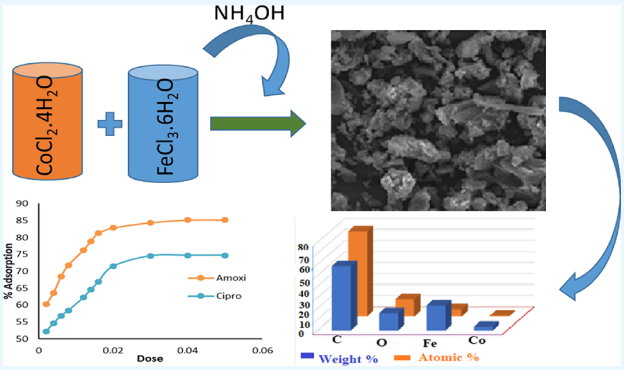

1. INTRODUCTION

A substance that is used to treat infection caused by a pathogen is called an antibiotic. Sometimes, it is also called antibacterial or antimicrobial medication.[1] We use antibiotics in the form of liquids, tablets, or capsules or via intravenous injection. For some skin infections, antibiotics can also be used in the form of creams, ointments, or lotions.[2] Different types of antibiotics are used such as Penicillin, Amoxicillin (Amoxi),[3−5] Tetracycline,[6−8] Lincomycins,[9,10] Sulfonamides,[11−13] Cephalosporin,[14,15] and Fluoroquinolones.[16,17] Some of them work by stopping the bacteria or parasite growth.[18,19]

Even though these medications have relatively low concentrations in water, their ongoing presence poses significant threats to the aquatic ecosystem and its microbes because of their cumulative effects.[20] Some common secondary effects in human beings are diarrhea, stomach discomfort, feeling ill, etc.[21−23] The most serious problem with antibiotic discharge into the environment is antibiotic resistance, which leads to failure in the therapeutic capability against infections in humans and animals. Antibiotic resistance is thought to be transmitted to the environment by human activities like fertilizer/biosolid application, wastewater irrigation, and agricultural use of antibiotic complexes.[24] However, investigations have discovered that soils already contain a broad and plentiful population of antibiotic-resistant bacteria.[25,26] Antibiotic contamination in the environment has the potential to be hazardous to microorganisms, plants, animals, and eventually humans. Toxicity, according to a popular belief, could be from the molecular level to the cellular, organism, individual, population, community, and finally ecosystem level.[27,28]

Drugs and pharmaceuticals have been acknowledged as entirely distinct marine environment divisions. Scientists are interested in removing medications and personal hygiene goods.[29] Urban treatment plants are unable to remove pharmaceutical chemicals from water due to their high solubility.[30] There are several attempts to remove antibiotics

Received: October 17, 2023
Revised: January 23, 2024
Accepted: January 26, 2024
Published: February 3, 2024

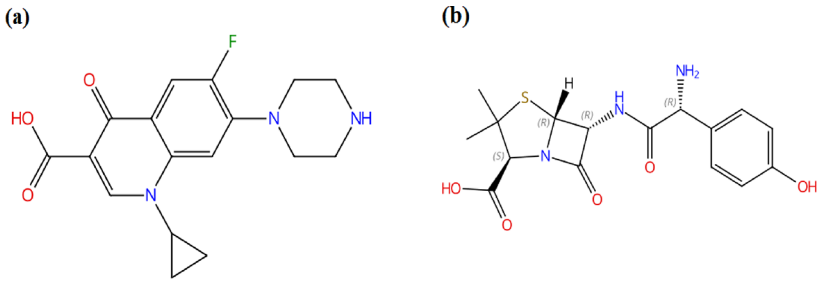

Figure 1. Structures of (a) ciprofloxacin and (b) amoxicillin.

in water using oxidation methods, potassium permanganate, ozone, Fenton's reagent, chlorine, etc.[31−33] Also, mineral composites and anaerobic and aerobic processes combined with ion exchange, chemical oxidation, coagulation-flocculation, irradiation, adsorption, precipitation, and membrane technologies are also used.[34] Consequently, there are several issues and disadvantages with all of these procedures, including their high cost, high solvent consumption, lengthy analytical times, difficult sample preparation, etc. The simplicity and ease of application of solid adsorbents make them the most successful among these approaches. Simple solid adsorbents however have many drawbacks, including a high price and poor selectivity.[35] Adsorption is a simple, efficient, less inexpensive, and less toxic method to remove pharmaceuticals (antibiotics) from water.[36,37] Different adsorbents can be used to fulfill this purpose including black cumin seeds (BCs), activated carbons (ACs), graphene natural clay compounds like bentonite, ion exchange materials, etc.[38,39] Out of these, adsorbents with nanoscale dimensions have gained attention due to their unique properties like greater chemical and mechanical stability, high enrichment and adsorption capacity, fast adsorption, etc. These and other properties of nanoparticles can be enhanced/improved by synthesizing the nanocomposites to obtain raised adsorption capacities.[20,29] Therefore, nanocomposites are growing rapidly due to their outstanding photocatalytic efficacy, ease of availability, long-term stability, and nontoxicity. Thus, nanocomposites have been considered for numerous applications such as in imaging, in biomedical devices including nanomedicines, and in heterogeneous catalysis.[40,41]

As far as we are aware, we have used for the very first time this activated carbon bimetallic nanocomposite (AC-$CoFe_2O_3$) for the adsorption of two pharmaceutical pollutants (Cipro and Amoxi) from water to increase the efficiency of the adsorption process and to drive the thresholds of nanocomposite adsorbents. This study covers different optimization studies like pH, contact time, adsorbent dose, concentration of antibiotics, and temperature as well. The mechanism of the adsorption process has been established by isotherm and kinetic modeling, and the feasibility of the process has been determined by applying thermodynamics.

2.0. METHODS AND MATERIALS

2.1. Materials. All solvents and antibiotics used were of analytical grade. Chemicals used in the research work included hydrochloric acid (HCl) (Riedelde Haen), ammonium hydroxide (NH_4OH), (Scharlau), sodium hydroxide (NaOH) (Riedelde Haen), cobalt-2-chloride tetrahydrate ($CoCl_2{\cdot}4H_2O$) (Riedel-de Haen), iron-6-chloride hexahydrate ($FeCl_6{\cdot}6H_2O$) (Scharlau), activated carbon (Riedelde Haen), and Cipro and Amoxi (SNB Pharmaceuticals Peshawar Pakistan). Water was obtained using a Millipore Milli-Q system. The structures of antibiotics are given in Figure 1.

2.2. Characterization of Carbon-Supported $CoFe_2O_3$. The morphology of the prepared nanocomposites was obtained by scanning electron microscopy (SEM) (JSM 5910, Jeol, Japan) at various magnifications of 500×, 1000×, 5000×, and 10,000×. A Fourier transform infrared (FTIR) spectroscope Vertex 70 (Bruker, Billerica, MA, USA) with a DLaTGS detector and a He Ne laser in the 4000−500 cm^{-1} range was used to examine the nanocomposite structure. On an automated pore size and surface area analyzer, the Brunauer−Emmett−Teller (BET) surface area and pore size distribution were calculated using N_2 adsorption−desorption (JW-BK122W, Beijing JWGB), an energy-dispersive X-ray (EDX) system (INCA200/Oxford Instruments) was used for elemental composition, and a UV−visible double beam spectrophotometer (Model SP-3000DB, Optima, Japan) was used for absorbance measurement using quartz cuvettes. The spectral bandwidth and wavelength range for this instrument is 1 nm and 190 to 1100 nm.

2.3. Synthesis of the Carbon-Supported $CoFe_2O_3$ Nanocomposite. A coprecipitation method was used to synthesize the carbon-supported $CoFe_2O_3$ nanocomposite. $CoCl_2{\cdot}4H_2O$ and $FeCl_3{\cdot}6H_2O$ were added in 1:2, respectively, and kept in distilled water with continuous stirring for 2 h at 343.15 K temperature. After that, ammonium solution (NH_4OH) (1.5 mol/L) was added dropwise to the previous flask until solidification. During base addition, activated carbon was also added from time to time to the solution. The precipitate was filtered and thoroughly washed many times with distilled water and dried at 423.15 K for 24 h to obtain an ultrafine precipitate.

2.4. Adsorption Studies of Cipro and Amoxi. A 100 ppm working solution of Cipro and Amoxi was used for the adsorption study. Each experiment was carried out by taking 10 mL of the solution in a conical flask, a buffer solution of the desired pH (2 and 12), and an appropriate adsorbent amount (0.04 g), and the solution was kept for the adsorption of Cipro and Amoxi for different intervals of time (10 min). After the adsorption, the adsorbent solution was filtered using Whatman filter paper to separate the adsorbent. Then, Cipro and Amoxi solutions were analyzed using an ultraviolet visible spectrophotometer (Model SP-3000DB) at 275 and 270 nm, respectively. The adsorption of Cipro and Amoxi was measured before and after the adsorption, and the percent (%) removal was calculated using the following formula:

$$\%\ \text{removal} = \frac{C_o - C_f}{C_o} \times 100 \quad (1)$$

https://doi.org/10.1021/acsomega.3c08161
ACS Omega 2024, 9, 6815−6827

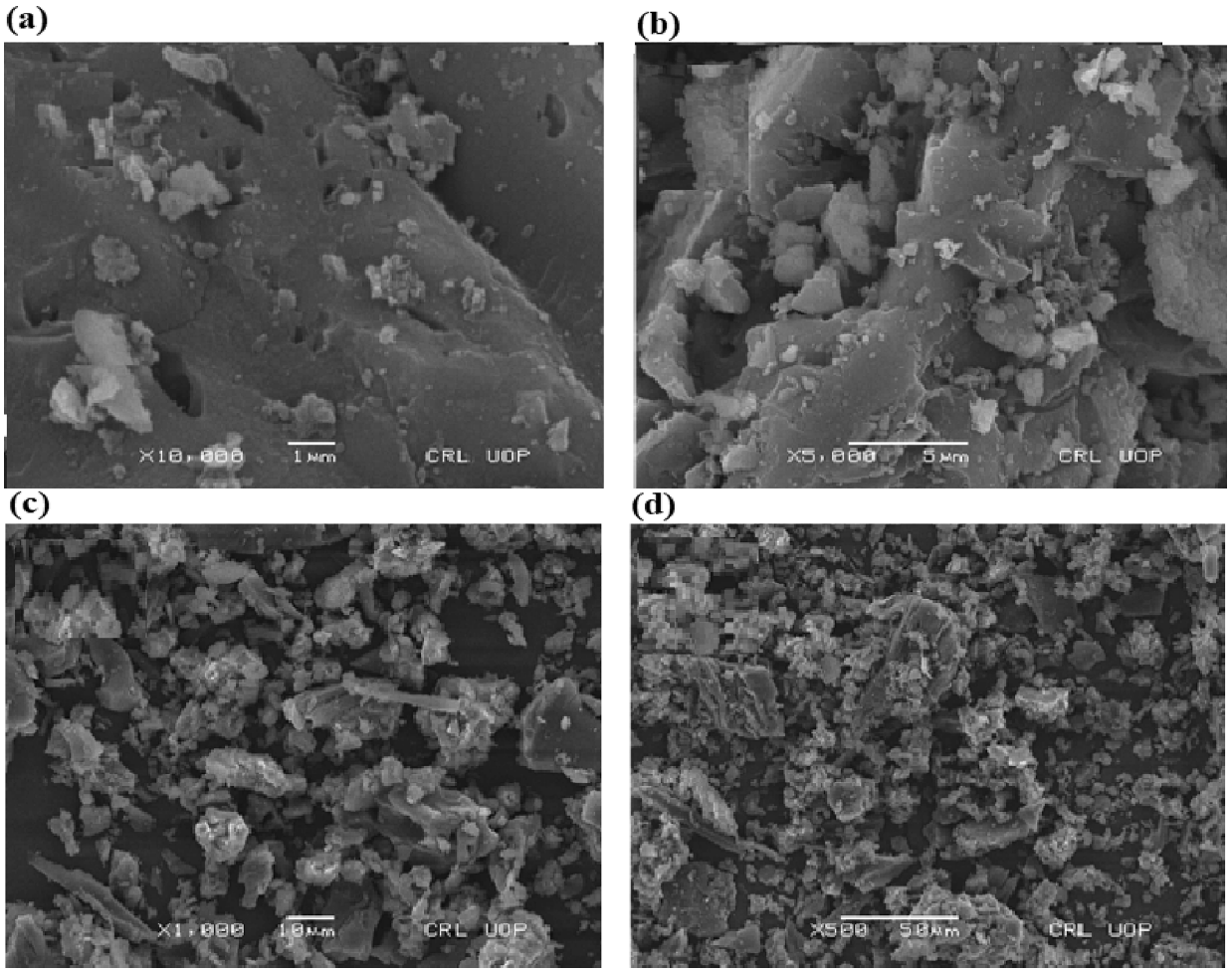

Figure 2. SEM images of AC-Co-Fe_2O_3 at various magnifications 500×, 1000×, 5000×, and 10000×. (a−d) Effective loading with cobalt and iron oxide.

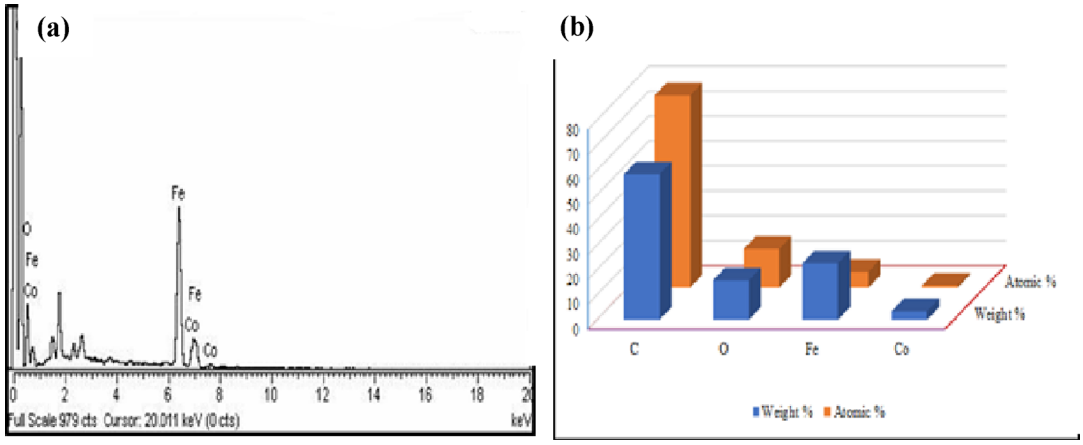

Figure 3. (a, b) The EDX pattern of AC-Co-Fe_2O_3 confirmed the presence of cobalt (Co), iron (Fe), oxygen (O), and carbon (C) at ratios of 60, 15, 22, and 2.8% by weight, respectively.

where C_o is the initial concentration and C_f is the final concentration.

2.5. Real Sample Analysis. Different natural water samples, namely, deionized water from the Millipore Milli-Q system, tap water from a chemical faucet in the University of Malakand, and river water from the river Swat, Chakdara KPK, Pakistan, were collected in prewashed polyethylene bottles. Tap and river water had suspended particles so they were allowed to settle for 24 h and then filtered using filter paper before analysis. The natural water samples were colorless having pH 6.5. These samples were analyzed for the presence of drugs (Cipro and Amoxi). Since no drug was found in these samples, spiking was carried out by adding known concentrations of drugs (100 mg/L). These spiked samples were then submitted to the optimum adsorption method to assess the application of the nanocomposite for the elimination of drugs (Cipro & Amoxi) from different types of

https://doi.org/10.1021/acsomega.3c08161
ACS Omega 2024, 9, 6815−6827

natural water samples. The capability of the nanocomposite to adsorb drugs from spiked water samples seemed to be impacted in tap water and river water because of the presence of dissolved organic and inorganic substances.

3.0. RESULTS AND DISCUSSION

3.1. Characterization of Synthesized AC-$CoFe_2O_3$. The synthesized nanocomposite was characterized by different techniques such as SEM, FT-IR, UV−visible spectrophotometry, EDX, and BET using scanning electron microscopy (SEM), by which size information and morphology can be obtained.[42] Figure 2 shows the SEM images of AC-Co-Fe_2O_3 at various magnifications 500×, 1000×, 5000× and 10,000×. These images clearly show that the surface of activated carbon was effectively loaded with cobalt and iron oxide and the bimetallic nanoparticles were homogeneously dispersed on the surface of activated carbon. The particle morphology was rough and irregular. Moreover, the particles were well structured having porous morphology.[43]

The EDX pattern of AC-Co-Fe_2O_3 as given in Figure 3 confirmed the presence of cobalt (Co), iron (Fe), oxygen (O), and carbon (C). The EDX pattern showed that C, O, Fe, and Co are present at ratios of 60, 15, 22, and 2.8% by weight, respectively, while by atomic ratio, C, O, Fe, and Co are 78, 15, 6, and 0.8%, respectively.[44] This shows that AC-Co-Fe_2O_3 was synthesized successfully.

FT-IR spectrum was used to analyze the surface functional groups of the $CoFe_2O_3$ nanocomposite in the range of 4000 to 400 cm^{-1}.[42] The stretching vibration at 3420 cm^{-1} in Figure 4

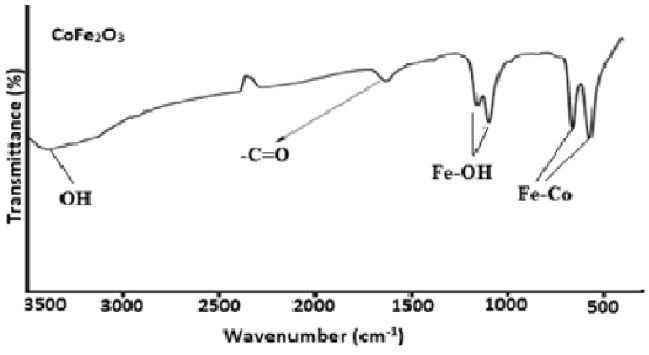

Figure 4. The FT-IR spectrum (500−4000 cm^{-1}) of the AC-$CoFe_2O_3$ nanocomposite confirmed the vibration at 3420 cm^{-1} of OH and bending vibrations of C=O at roughly 1639 and 1489 cm^{-1}, while the Fe−Co stretching mode bands may be seen at 661, 609, and 583 cm^{-1}.

indicates the presence of OH on the surface of cobalt ferrite. The asymmetric and symmetric bending vibrations of C=O were seen at maxima at roughly 1639 and 1489 cm^{-1}. The Fe−Co stretching mode bands may be seen at 661, 609, and 583 cm^{-1}.[45]

The Brunauer−Emmett−Teller (BET) equation was applied to the resulting nitrogen physisorption data to produce multilayer adsorption isotherm plots, which were then used to calculate the specific pore volume, pore size, and surface area of the nanocomposite sample. The BET plots in Figure 5 show the average surface area (116 $m^2\ g^{-1}$) and pore volume (0.19 $cm^3\ g^{-1}$), and the average values of pore diameter of the parent AC-$CoFe_2O_3$ nanocomposite (27 Å) are also given in Table 1. The International Union of Pure and Applied Chemistry (IUPAC) designated the BET isotherms of the nanocomposites as type II adsorption isotherms since they showed an H3 hysteresis loop. It is a property of mesoporous materials whose mesoporous volumes are poorly defined due to the aggregate nanocomposites' nonrigid structure and low-degree pore curvature.[46,47]

3.3. Effect of pH. The adsorption studies of Cipro and Amoxi were carried out at variable pH values from 2 to 13 with 30 min contact time, 0.002 g of adsorbent weight, and 10 mL of 100 $\mu g\ mL^{-1}$ Cipro solution at room temperature. First, a decrease in adsorption was observed until pH 7, then adsorption increased at a higher pH, and maximum adsorption occurred at pH 12. At pH levels higher than 12, adsorption remained constant. With the change in pH, ionization of Cipro occurred. Ciprofloxacin has a positive charge, which favored electrostatic repulsion in acidic solution, which made adsorption difficult. At a lower pH, it acted as a cation, and at a higher pH, it behaved as an anion. Due to this ionization and metal bridging as well, the maximum adsorption of Cipro occurred at pH 12, which was 74.58%.[48] The percent adsorption is shown in Figure 6a. For Amoxi, similar experiments were performed, and the maximum adsorption of 48.31% took place at pH 2. Amoxicillin was negatively charged, and the anionic group was largely possible to be bound by the positively charged metal through electrostatic interactions and cation exchange.

3.4. Effect of Adsorbent Dose. Investigation of the optimum amount of adsorbent for maximum adsorption is of vital importance in adsorption studies as it determines the cost effectiveness of the developed method and adsorption capacity of the adsorbent per used amount. Therefore, this study was carried out by changing the weight of AC-$CoFe_2O_3$ from 0.002 to 0.06 g keeping other parameters constant like pH (12), contact time (30 min), and volume (10 mL of Cipro working solution) at room temperature. When with an increase in dosage, the surface area of adsorbent increases for adsorbate and also more active sites of adsorbent become available for adsorption. For Cipro, the maximum adsorption occurred at 0.04 g, and then, no change in adsorption was observed with an increase in dosage. The graph between adsorbent dose and percent adsorption is shown in Figure 6b. Adsorption of Amoxi also increased with an increase in adsorbent dose due to the increased pores of adsorbent, and the maximum adsorption was noticed at 0.016 g, so 0.016 g was taken as the optimum dose to carry out further experiments. The data is shown in Figure 6b.

3.5. Effect of Contact Time. The effect of time on the adsorption of Cipro using AC-$CoFe_2O_3$ was investigated at the optimized parameters of pH 12 and adsorbent dose (0.04 g). The contact time was varied from 10 to 100 min with a time interval of 10 min. With an increase in contact time, adsorption was enhanced due to an increase in the interaction of sorbate with adsorbent active sites, and maximum adsorption was obtained at 80 min (95.03 and 82.82% for Cipro and Amoxi, respectively). The effect of contact time on adsorptions is shown in Figure 6c for Cipro and Amoxi.

3.6. Effect of Temperature. To study the effect of temperature on the adsorption of Cipro and Amoxi, the temperature was varied from 293 to 333 K with a 10 K interval. Other parameters were kept constant, such as pH (12), contact time (80 min), adsorbent dose (0.04 g), and volume (10 mL) of Cipro and Amoxi. With an increase in temperature, the % adsorption increased and maximum % adsorption was obtained at 333 K, which was 98.41 and 89.09% for Cipro and Amoxi, respectively. Data obtained from temperature effect on % adsorption of Cipro and Amoxi is shown in Figure 6d.

https://doi.org/10.1021/acsomega.3c08161
ACS Omega 2024, 9, 6815−6827

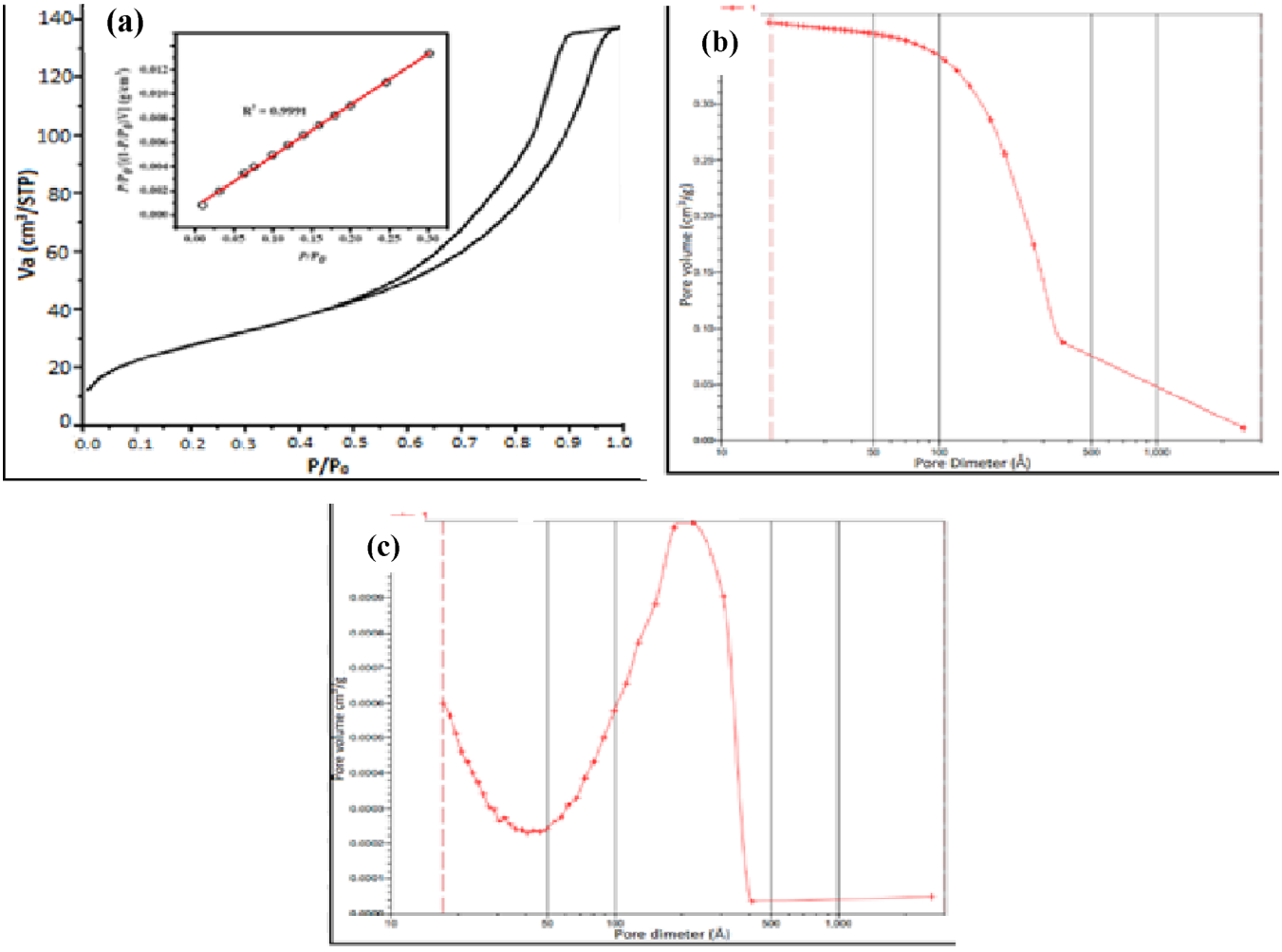

Figure 5. BET graphs showing the (a) N_2 adsorption−desorption isotherm and (b, c) pore volume of the AC-$CoFe_2O_3$ nanocomposite.

Table 1. BET Study of the Carbon-Supported Nanocomposite (AC-$CoFe_2O_3$)

adsorbent	specific surface area	pore volume	pore radius
AC-$CoFe_2O_3$	116 $m^2\ g^{-1}$	0.19 $cm^3\ g^{-1}$	27 Å

3.7. Adsorption Kinetics. Adsorption kinetics was investigated at three different temperatures for Cipro and Amoxi by modeling kinetic data using different kinetic models like pseudo-first-order, pseudo-second-order, and intraparticle diffusion models. This modeling of kinetic data was carried out for determination of a precise adsorption mechanism and possible rate-limiting step during the adsorption process.[49] For this purpose, 0.04 and 0.016 g of AC-Co-Fe_2O_3 were added to a series of 10 mL flasks containing 0.1 ppm Cipro and Amoxi, respectively. Analysis of experimental data at different intervals made it possible to calculate the kinetic parameters and design and model the adsorption process to obtain certain informations.[50] Figure 7 shows these information about the kinetics adsorption of Cipro and Amoxi.

3.7.1. Pseudo-First-Order Kinetic Model. The linear form of the pseudo-first-order kinetic equation is as follows:

$$\ln(q_e - q_t) = \ln q_e - k_1 \times t \quad (2)$$

In eq 2, q_e is the adsorption of drugs (mg g^{-1}) at equilibrium time, while q_t is the adsorption at any time (min), and k_1 is a first-order constant. By using the graph of $\log(q_e - q_t)$ against "t", we calculated k_1 (min^{-1}). Figure 8a,b shows the pseudo-first-order kinetics at different temperatures (293, 313, and 333 K), whereas various parameters are given in Table 2. The experimental q_e and calculated q_e do not match each other, and also, the correlation coefficient R^2 for both adsorption processes is less than 0.99, so this model is not applicable; thus, the adsorption of Cipro and Amoxi is not physical.

3.7.2. Pseudo-Second-Order Model. The pseudo-second-order model can be described using eq 3

$$\frac{t}{q_t} = \frac{1}{k_2 q_e^2} + \frac{t}{q_e} \quad (3)$$

where q_e is the adsorption at equilibrium time while q_t is the adsorption at any time, "t" is the contact time, and k_2 is a pseudo-second-order constant. The k_2 (g mg^{-1} min^{-1}) and correlation coefficient R^2 values for the adsorption process of Cipro and Amoxi on AC-Co-Fe_2O_3 are tabulated in Table 2. The slope and conjunctions of the t/q_t versus "t" can be used to calculate the values of q_e (mg g^{-1}) and k_2.[51] The plot using eq 3 for Cipro and Amoxi at different temperatures (293, 313, and 333 K) is shown in Figure 8c,d, and data are given in Table 2. For both Cipro and Amoxi, R^2 values are closest to 1 and experimental q_e is close to calculated q_e; therefore, the best model to describe the adsorption process is the pseudo-second-order model showing the chemical nature of adsorption.

https://doi.org/10.1021/acsomega.3c08161
ACS Omega 2024, 9, 6815−6827

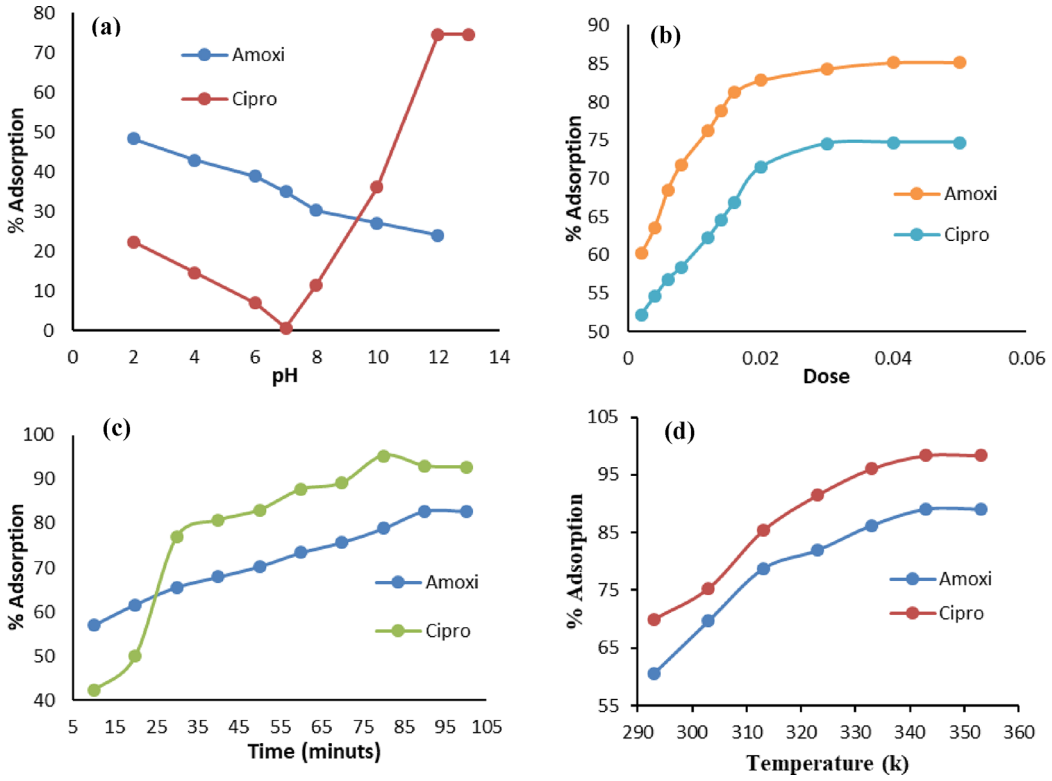

Figure 6. Effect of (a) pH from 2 to 13 with 30 min contact time, 0.002 g of adsorbent (AC-$CoFe_2O_3$), and 10 mL of 0.1 ppm Cipro and Amoxi with maximum adsorptions of 74.58% at pH 12 and 48.31% at pH 2, respectively, (b) dose, (c) contact time, and (d) temperature.

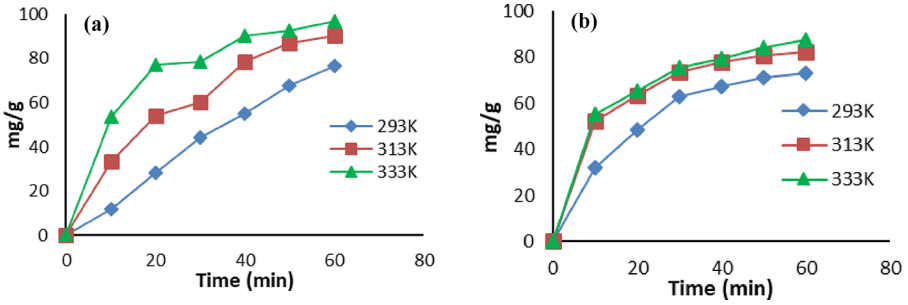

Figure 7. Kinetics adsorption at 0.04 and 0.016 g of AC-Co-Fe_2O_3 in 10 mL flasks containing 0.1 ppm (a) ciprofloxacin and (b) amoxicillin, respectively, at various temperatures (293, 313, and 333 K) with different intervals of time.

The examination of different parameters obtained from pseudo-first-order and pseudo-second-order kinetic models, i.e., R^2 values and maximum adsorption capacity, and also due to possible ionization of drugs, it can be suggested that chemisorption was the dominant mechanism for drug adsorption onto the nanocomposite. But, since the R^2 value for the pseudo-first-order was greater than 0.9, this model can also not be ignored. So in the end, we can suggest that adsorption of drugs onto the nanocomposite involved both physical and chemical processes.[52]

3.7.3. Intraparticle Diffusion Model. The mathematical form of the intraparticle diffusion model is as follows:

$$q_t \; k_{id} t^{\frac{1}{2}} + \; C \tag{4}$$

where k_{id} is the intraparticle diffusion constant and C shows the thickness of the boundary layer. The intraparticle plot of time vs t/q_t is shown in Figure 8e,f for Cipro and Amoxi at 293, 313, and 333 K, respectively, and data is given in Table 2. The boundary effect will be greater if the intercept value is greater, and if the line passes through the origin, there will be incorporation of the intraparticle diffusion model and the intraparticle diffusion will be a controlling step. If it does not go beyond the origin, it can be concluded that not only the intraparticle distribution but also the boundary layer (film distribution) has some effect on the rate-controlling phase.[53]

3.8. Effect of Concentration. The effect of Cipro and Amoxi concentration using Ac-$CoFe_2O_3$ was studied at different concentrations, i.e., from 100 to 450 ppm. The adsorption efficiency decreases with an increase in concentration because the active sites of adsorbent become occupied, and no further site is available for adsorption of more adsorbate. The % adsorption Cipro (a) and Amoxi (b) vs concentration is shown in Figure 9.

3.9. Isotherm Study. For additional features like whether the adsorption of drugs was a monolayer or multilayer onto the nanocomposite and adsorbent compatibility of adsorbate, different isotherm models such as Langmuir, Freundlich, and

https://doi.org/10.1021/acsomega.3c08161
ACS Omega 2024, 9, 6815−6827

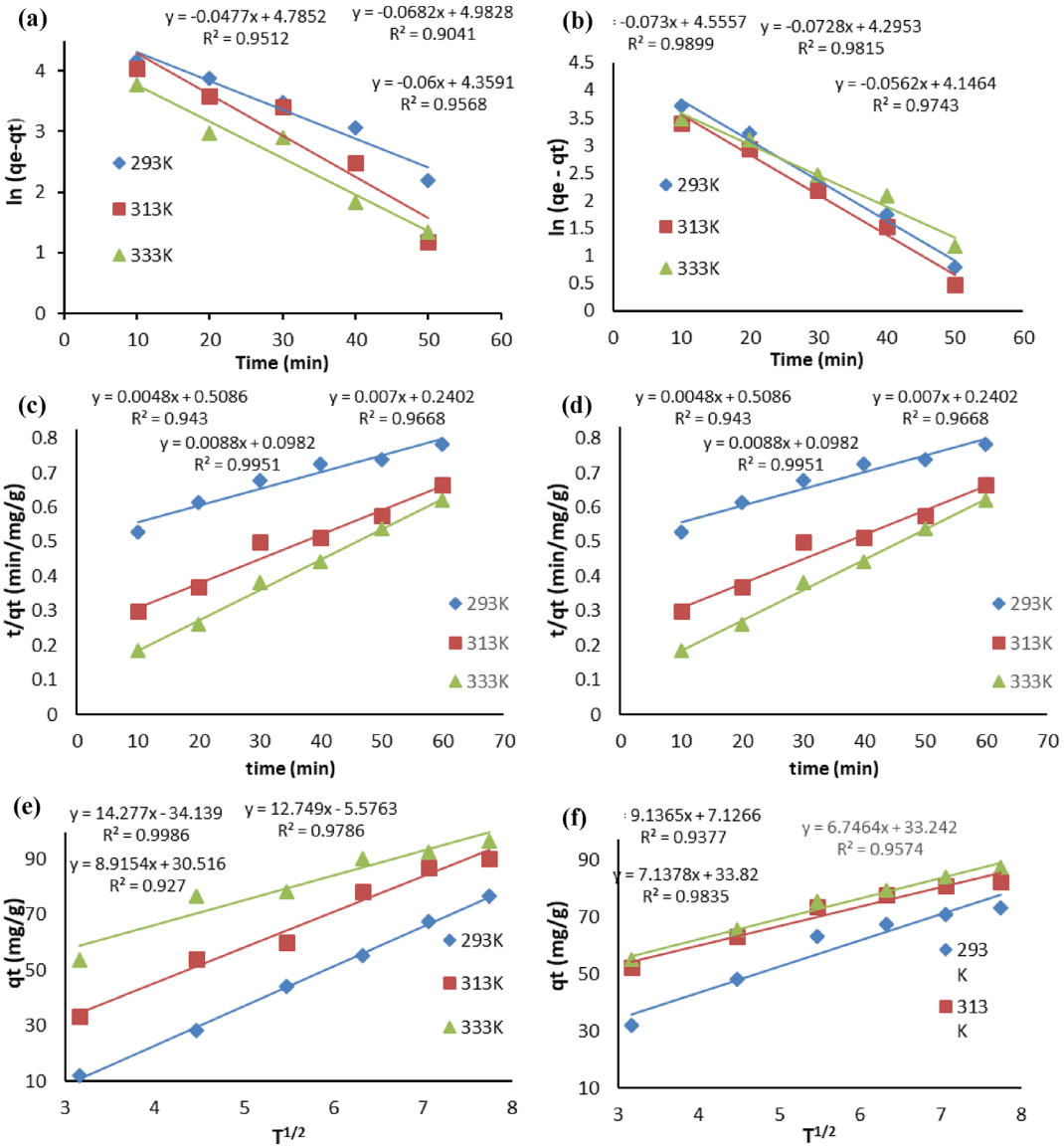

Figure 8. (a) Pseudo-first-order, (c) pseudo-second-order, and (e) intraparticle models for ciprofloxacin and (b) pseudo-first-order, (d) pseudo-second-order, and (f) intraparticle models for adsorption of amoxicillin at different temperatures 293, 313, and 333 K.

Table 2. Kinetics Model Parameters for Drug Adsorption

	ciprofloxacin			amoxicillin		
parameter	293 K	313 K	333 K	293 K	313 K	333 K
Pseudo-first-order						
q_e (cal) (mg/g)	119.2	145.75	78.12	63.15	73.27	95.21
k_1 (min^{-1})	0.0477	0.0682	0.06	0.056	0.0728	0.0713
R^2	0.9512	0.904	0.9568	0.09743	0.9815	0.9899
Pseudo-second-order						
q_e (cal) (mg/g)	113.6	142.85	208.04	94.02	100.12	100.9
k_2 (g/mg/min)	0.00032	0.00049	0.00067	0.00049	0.0015	0.00107
R^2	0.9981	0.9668	0.943	0.9974	0.999	0.9924
Intraparticle diffusion model						
k_{id}	14.2771	12.749	8.918	9.136	6.7464	7.137
C	34.139	5.576	30.516	7.12	33.24	33.82
R^2	0.9986	0.9786	0.927	0.9377	0.9574	0.9835

Tempkin were applied at different temperatures (293, 313, and 333 K) to study the adsorbent surface monolayer or multilayer.[45]

3.9.1. Langmuir Isotherm Model. To explain the mechanism of adsorption of Cipro and Amoxi on the adsorbent, this model was successfully applied. The basic assumption of this model is

https://doi.org/10.1021/acsomega.3c08161
ACS Omega 2024, 9, 6815−6827

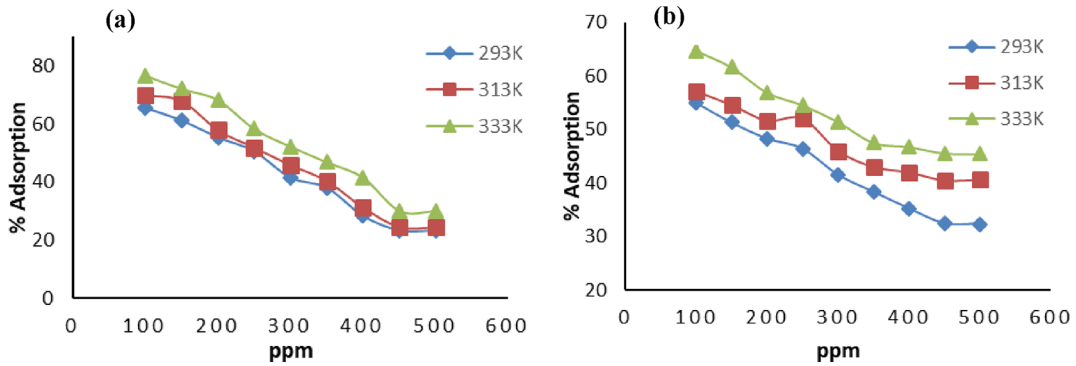

Figure 9. Effect of Cipro and Amoxi concentrations (100−450 ppm) on the adsorption on Ac-$CoFe_2O_3$: % of adsorption of (a) Cipro and (b) Amoxi at different temperatures (293, 313, and 333 K).

Table 3. Different Isotherm Parameters for Adsorption of Drugs (Cipro and Amoxi) onto the Nanocomposite

	ciprofloxacin			amoxicillin		
parameters	293 K	313 K	333 K	293 K	313 K	333 K
			Langmuir isotherm model			
Q_m (mg/g)	125	166.6	312.6	192	196.07	217.76
K_L (L/mg)	3.63	0.1609	0.107	0.4727	0.1841	0.268
R^2	0.9937	0.9887	0.9559	09683	0.9951	0.9966
			Freundlich isotherm model			
$1/n$	0.0412	0.1006	0.1392	0.0734	0.1557	0.1148
K_f (L/mg)	104.007	95.56	95.30	92.81	89.36	1.0938
R^2	0.1737	0.7302	0.8576	0.496	0.7979	0.5088
			Temkin isotherm model			
B_1	4.2298	12.76	19.706	8.19	21.928	15.758
K_T(L/mg)	13.05	2.11	1.578	8359.82	41.007	1226.52
R^2	0.1374	0.743	0.8586	0.4835	0.8403	0.4755

that the adsorption process takes place at certain homogeneous sites contained by the adsorbent. The model can be mathematically expressed as

$$\frac{C_e}{q_e} = \frac{C_e}{Q_m} + \frac{1}{K_L Q_m} \quad (5)$$

where C_e, K_L, and Q_m are the liquid-phase equilibrium concentrations of drugs (mg L^{-1}), Langmuir constant (L g^{1-}), and bulk dosage of adsorption (mg g^{-1}), respectively.[45] The plot of C_e/q_e vs C_e must be linear with an intercept ($1/Q_mK_L$) and slope $1/Q_m$. As shown in Table 3, the maximum adsorption capacities of the nanocomposite is 312.6 and 217.76 mg g^{-1}, and Figure 10a,b shows the models for Cipro and Amoxi, respectively, at 333 K, while Figure S1a−d shows the model at 293 and 313 K. The R^2 values 0.95 and 0.99 of the model indicate that Langmuir is the best model for defining the correct adsorption process.

3.9.2. Freundlich Isotherm Model. This model shows adsorption that may be an inappropriate retrofit and is not limited to monolayer production. This model can be expressed as

$$\ln q_e = \ln K_f + \frac{1}{n} \ln C_e \quad (6)$$

where C_e (mg L^{-1}) shows the liquid phase concentration at equilibrium, q_e (mg g^{-1}) indicates the adsorption of drugs, while K_f (mg g^{-1}) is the relative adsorption capacity. On the other hand, $1/n$ determines the heterogeneity factor of the surface for drug adsorption. The $1/n$ value should be less than 1 for best adsorption, while it will be higher than 1 for worst adsorption.[54]

Therefore, $1/n$ values are 0.1392 and 0.1148 for Cipro and Amoxi, respectively, indicating that the adsorption process is favorable. Figure 10c,d shows the Freundlich model of Cipro and Amoxi at 333 K, respectively, and Figure S2e−h shows the model at 293 and 313 K. Various parameters are given in Table 3.

3.9.3. Temkin Isotherm Model. This model can be expressed as

$$q_e = \beta \ln K_T + \beta \ln C_e \quad (7)$$

where $\beta = RT/b$ is related to the adsorption temperature, T is the total Kelvin temperature, and R (J mol^{-1} K^{-1}) is a gas constant.[31] The structure against ln C_e enabled us to determine the values of these fixed parameters. Figure 10e,f shows the Tempkin isotherm adsorption of Amoxi and Cipro at 333 K onto AC-Co-Fe_2O_3, respectively, while Figure S3i−l shows the model at 293 and 313 K. As can be seen in Table 3, in contrast to the Freundlich and Temkin models, the regression values and adsorption capacities for Cipro and Amoxi are greater for the Langmuir isotherm. Therefore, based on these results, we can suggest that the adsorption of Cipro and Amoxi better followed the Lamgmuir isotherms as compared to the other isotherms.

3.10. Thermodynamic Study. The relationship between thermodynamic parameters like Gibbs free energy, enthalpy, and entropy with respect to temperature was attained for the adsorption of Cipro and Amoxi onto AC-$CoFe_2O_3$ by performing thermodynamic studies at three different temperatures.[55] The parameters were calculated using eqs 8 and 9

https://doi.org/10.1021/acsomega.3c08161
ACS Omega 2024, 9, 6815−6827

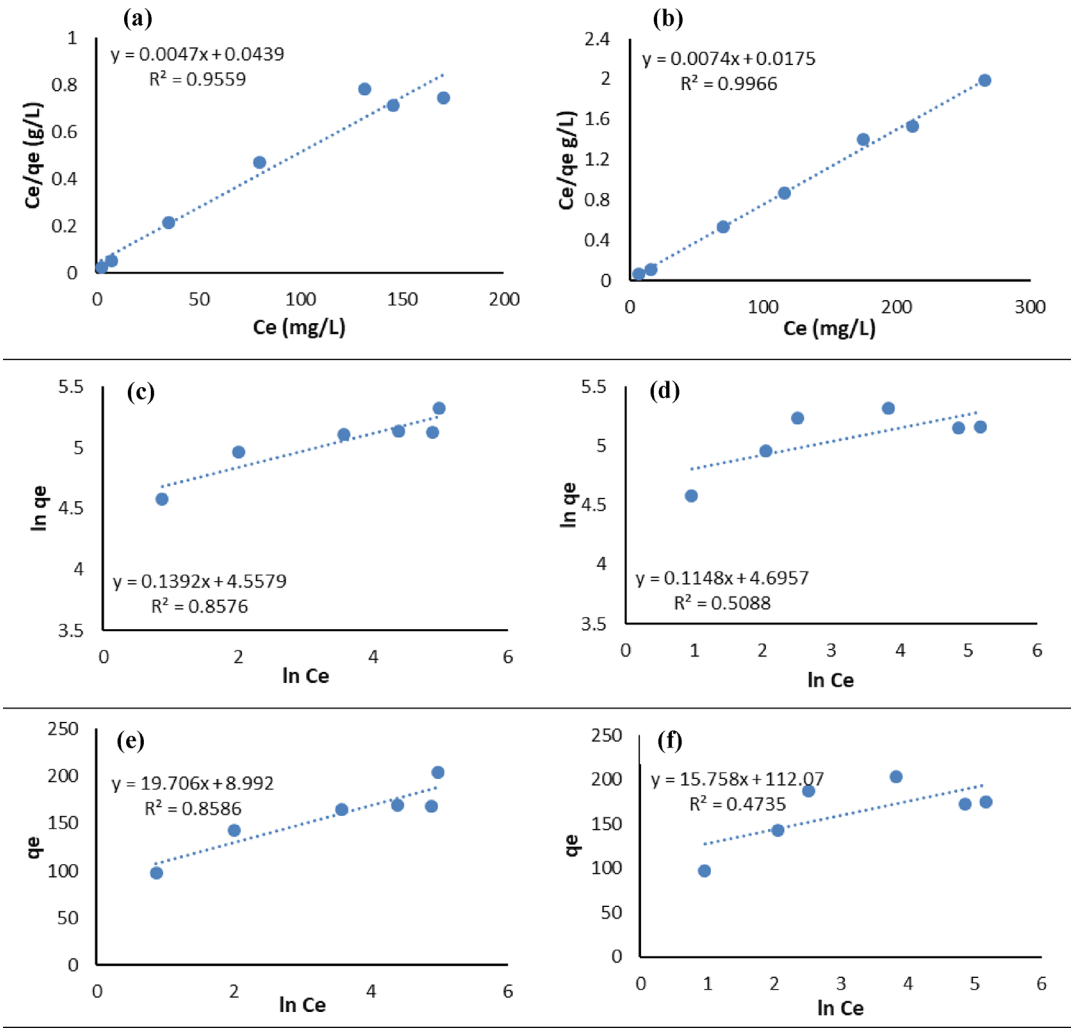

Figure 10. (a, b) Langmuir, (c, d) Freundlich, and (e, f) Temkin isotherm models for the adsorption of Ciprofloxacin and Amoxicillin, respectively, at 333 K.

$$\ln(K_c) = \frac{\Delta S^\circ}{R} - \frac{\Delta H^\circ}{RT} \quad (8)$$

$$\Delta G^\circ = \Delta H^\circ - T\Delta S^\circ \quad (9)$$

where K_c (Lg^{1-}) is the thermodynamic equilibrium constant represented by q_e/C_e, T (K) is the absolute temperature, and R (8.314 J $mol^{-1}K^{-1}$) is the universal gas constant. The intercept and slope of a plot log K_c vs $1/T$ were used to calculate the values of ΔS° and ΔH°. Different parameters were studied at various temperatures listed in Table 4, and the van't Hoff plot is displayed in Figure 11. At all temperatures, the Gibbs free energy change (ΔG°) was negative, indicating that the adsorption of Cipro and Amoxi is spontaneous and feasible. The positive value ΔH° indicated that the present study adsorption process is endothermic because the rising temperature caused the increase in the rate of adsorbate diffusion on the adsorbents (external and internal surfaces). During adsorption, a positive change in entropy (ΔS °) indicated an increased disorderedness in the adsorption.

Table 4. Thermodynamic Parameters for Adsorption of Cipro and Amoxi

	ΔG° (kJ mol^{-1})		ΔH° (kJ mol^{-1})		ΔS° (J mol^{-1} K^{-1})	
temperature (K)	Cipro	Amoxi	Cipro	Amoxi	Cipro	Amoxi
293	−0.915	−0.674	28.092	19.836	99.9	70
313	−0.317	−2.074				
333	−0.517	−3.474				

3.11. Real Sample Analysis. For real sample application, deionized water, tap water, and river samples were employed to test the capability of this nanocomposite in eliminating Cipro and Amoxi. Deionized water was taken by using the Millipore Milli-Q system, tap water was obtained from a chemical faucet in the University of Malakand, and river water was obtained from river Swat, KPK, Pakistan, to assess how well the nanocomposite would recover the drugs Cipro and Amoxi from environmental samples. For the collected water for real sample analysis, the pH of river water was 7.4, with a density of 1.03 g/cm^3, while the pH of tap water was 6.5 with a density of 0.99 g/cm^3. The density was measured using a density meter (pycnometer), and the interferences were removed by filtration (Whatman filter paper). The samples were submitted to the optimized extraction procedure (pH 12 and 2) after being spiked with known concentrations of the drugs (100 mg/L) Cipro and Amoxi, and the nanocomposite showed efficiencies of 98 and 89%, respectively. Tap water and river water appear to have an

https://doi.org/10.1021/acsomega.3c08161
ACS Omega 2024, 9, 6815−6827

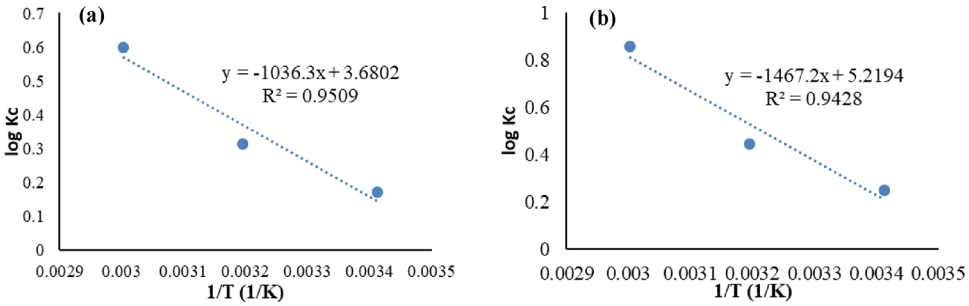

Figure 11. Plot $1/T$ vs log K_c for adsorption of (a) Cipro and (b) Amoxi.

impact on the nanocomposite's ability to adsorb drugs. The dissolved organic and inorganic materials in the river water samples marginally decreased the selective efficacy of the nanocomposite. Table 5 summarizes the results of drug (Cipro and Amoxi) adsorption from several water samples.

Table 5. Real Sample Analysis for the Adsorption of Cipro and Amoxi

samples	drugs	amount of drug added (mg/L)	amount of drug found (mg/L)	%recovery ± SD
deionized water	ciprofloxacin	100	98.41	98.40 ± 0.9
tap water		100	82.07	82.06 ± 1.20
river water		100	61.08	61.06 ± 0.34
deionized water	amoxicillin	100	89.09	89.08 ± 0.2
tap water		100	65.75	65.73 ± 0.6
river water		100	43.65	43.64 ± 0.4

3.12. Efficiency of the Synthesized Nanocomposites.

Table 6 presents a comparison between the adsorbent developed in this work and the existing adsorbents found in the literature. The comparison is based on the adsorption capacity, calculated using the Langmuir isotherm, for Cipro and Amoxi. The table clearly indicates that the synthesized nanocomposites exhibit a higher adsorption capacity compared to the already reported adsorbents. This demonstrates the superior effectiveness of the developed adsorbent for the removal of Cipro and Amoxi.

4.0. CONCLUSIONS

The focus of the present study was to synthesize nanocomposites (AC-$CoFe_2O_3$) and use them for the very first time as a new adsorbent to adsorb drugs (Cipro and Amoxi) from water. The carbon-supported nanocomposite AC-$CoFe_2O_3$ was synthesized using the coprecipitation method. Various parameters were optimized, such as time, pH, dose, temperature, and concentration for maximum adsorption. The efficacy of the adsorption process improved to 98.41 and 89.09% for Cipro and Amoxi, respectively, with an increase in dosage and time of contact. Different kinetic and isotherm models at various temperatures (293, 313, and 333 K) were applied to study the adsorption mechanism. The drug (Cipro and Amoxi) adsorption followed the pseudo-second-order kinetic and Langmuir models, thus indicating chemisorption. From the thermodynamic study, the negative value of ΔG° showed that the process is spontaneous, while ΔS° and ΔH° determined the feasibility and endothermic nature of the process, respectively.

Table 6. Comparison of Different Adsorbents for the Adsorption of Cipro and Amoxi Drugs

adsorbents	drugs	adsorption capacity (mg/g)	references
magnetic N-doped porous carbon	ciprofloxacin	1564	56
nickel sulfide nanomaterial		971.8	57
silica-based alginic acid		426.6	58
magnetic chitosan/graphene oxide		282.9	59
magnetite-imprinted chitosan		142.9	60
sodium alginate/graphene oxide		100.0	61
Fe_3O_4/carbon		90.10	62
Cu-glutamate MOF		61.35	63
bentonite-chitosan nanocomposite		39.06	64
carbon-supported nanocomposite (ACo-Fe_2O_3)		312.17	current study
activated carbon prepared from *Azolla filiculoides*	amoxicillin	265.2	65
activated carbon		163.93	66
magnetically modified graphene nanoplatelets		106.38	67
palm bark		35.92	68
tartaric acid-modified wheat grains		31.25	69
natural phosphate rock (francolite)		23.3	70
carbon-supported nanocomposite (ACo-Fe_2O_3)		217.76	current study

Therefore, it can be concluded that Ac-Co-Fe_2O_3 is a good choice for the adsorption of antibiotics (Cipro and Amoxi) and this research can be further expanded to adsorb other drugs as well for other applications too.

■ ASSOCIATED CONTENT

Data Availability Statement

All concerned data is given in this manuscript.

Supporting Information

The Supporting Information is available free of charge at https://pubs.acs.org/doi/10.1021/acsomega.3c08161.

Langmuir, Freundlich, and Temkin isotherm models for the adsorption of Ciprofloxacin and Amoxicillin at 293 and 313 K (PDF)

https://doi.org/10.1021/acsomega.3c08161
ACS Omega 2024, 9, 6815−6827

AUTHOR INFORMATION

Corresponding Author

Muhammad Zahoor − *Department of Biochemistry, University of Malakand, Chakdara, Khyber Pakhtunkhwa 18000, Pakistan;* orcid.org/0000-0002-4528-8517; Email: mohammadzahoorus@yahoo.com

Authors

Maria Sadia − *Department of Chemistry, University of Malakand, Chakdara 18800, Pakistan*

Izaz Ahmad − *Department of Chemistry, University of Malakand, Chakdara 18800, Pakistan; Department of Chemistry and Chemical Technology, Al-Farabi Kazakh National University, Almaty 050040, Kazakhstan*

Shaukat Aziz − *Department of Chemistry, University of Malakand, Chakdara 18800, Pakistan*

Rizwan Khan − *Department of Electrical Engineering, Kwangwoon University Seoul, Seoul 54047, South Korea*

Riaz Ullah − *Department of Pharmacognosy, College of Pharmacy, King Saud University, Riyadh 11451, Saudi Arabia;* orcid.org/0000-0002-2860-467X

Essam A. Ali − *Department of Pharmaceutical Chemistry, College of Pharmacy King Saud University Riyadh, Riyadh 11451, Saudi Arabia*

Complete contact information is available at: https://pubs.acs.org/10.1021/acsomega.3c08161

Author Contributions

M.S.: methodology, visualization, conceptualization, supervision, writing and editing original draft. I.A.: writing original draft, visualization, investigation. S.A.: methodology. R.K.: review and editing. M.Z.: conceptualization, write up original draft. R.U. and E.A.A.: methodology, investigation, visualization, investigation, and resources.

Notes

The authors declare no competing financial interest.
All authors declare that the described work is original.
This study is not violating any ethical rules.
Not applicable.
All authors highly agree to submit this work for publication.

ACKNOWLEDGMENTS

The authors extend their appreciation to the researchers supporting Project Number (RSP2024R110) King Saud University, Riyadh, Saudi Arabia, for financial support.

REFERENCES

(1) Hu, X.-Y.; Zhou, K.; Chen, B.-Y.; Chang, C.-T. Graphene/TiO2/ZSM-5 Composites Synthesized by Mixture Design Were Used for Photocatalytic Degradation of Oxytetracycline under Visible Light: Mechanism and Biotoxicity. *Appl. Surf. Sci.* **2016**, *362*, 329−334.

(2) Hauser, W. E.; Remington, J. S. Effect of Antibiotics on the Immune Response. *Am. J. Med.* **1982**, *72* (5), 711−716.

(3) Ligon, B.; Penicillin, L. Its Discovery and Early Development. *Semin Pediatr Infect Dis* **2004**, *15* (1), 52−57.

(4) Banks, T. A.; Tucker, M.; Macy, E. Evaluating Penicillin Allergies Without Skin Testing. *Curr. Allergy Asthma Rep* **2019**, *19* (5), 27.

(5) Trubiano, J. A.; Adkinson, N. F.; Phillips, E. J. Penicillin Allergy Is Not Necessarily Forever. *JAMA* **2017**, *318* (1), 82−83.

(6) Daghrir, R.; Drogui, P. Tetracycline Antibiotics in the Environment: A Review. *Environ. Chem. Lett.* **2013**, *11* (3), 209−227.

(7) Chopra, I.; Roberts, M. Tetracycline Antibiotics: Mode of Action, Applications, Molecular Biology, and Epidemiology of Bacterial Resistance. *Microbiol Mol. Biol. Rev.* **2001**, *65* (2), 232−260.

(8) Nguyen, F.; Starosta, A. L.; Arenz, S.; Sohmen, D.; Dönhöfer, A.; Wilson, D. N. Tetracycline Antibiotics and Resistance Mechanisms. *Biol. Chem.* **2014**, *395* (5), 559−575.

(9) Jamal, M.; Shareef, M.; Sajid, S. Lincomycin and Tetracycline Resistance in Poultry. Review. *Matrix Science Pharma (MSP)* **2017**, *1* (1), 33−38.

(10) Zhanel, G. G.; Dueck, M.; Hoban, D. J.; Vercaigne, L. M.; Embil, J. M.; Gin, A. S.; Karlowsky, J. A. Review of Macrolides and Ketolides. *Drugs* **2001**, *61* (4), 443−498.

(11) Wegst-Uhrich, S. R.; Navarro, D. A.; Zimmerman, L.; Aga, D. S. Assessing Antibiotic Sorption in Soil: A Literature Review and New Case Studies on Sulfonamides and Macrolides. *Chem. Cent J.* **2014**, *8* (1), 5.

(12) Peiris, C.; Gunatilake, S. R.; Mlsna, T. E.; Mohan, D.; Vithanage, M. Biochar Based Removal of Antibiotic Sulfonamides and Tetracyclines in Aquatic Environments: A Critical Review. *Bioresour. Technol.* **2017**, *246*, 150−159.

(13) Dmitrienko, S. G.; Kochuk, E. V.; Apyari, V. V.; Tolmacheva, V. V.; Zolotov, Y. A. Recent Advances in Sample Preparation Techniques and Methods of Sulfonamides Detection − A Review. *Anal. Chim. Acta* **2014**, *850*, 6−25.

(14) Nightingale, C. H.; Greene, D. S.; Quintiliani, R. Pharmacokinetics and Clinical Use of Cephalosporin Antibiotics. *J. Pharm. Sci.* **1975**, *64* (12), 1899−1926.

(15) Thompson, R. L.; Wright, A. J. Cephalosporin Antibiotics. *Mayo Clin. Proc.* **1983**, *58* (2), 79−87.

(16) Riaz, L.; Mahmood, T.; Khalid, A.; Rashid, A.; Ahmed Siddique, M. B.; Kamal, A.; Coyne, M. S. Fluoroquinolones (FQs) in the Environment: A Review on Their Abundance, Sorption and Toxicity in Soil. *Chemosphere* **2018**, *191*, 704−720.

(17) Scoper, S. V. Review of Third-and Fourth-Generation Fluoroquinolones in Ophthalmology: In-Vitro and in-Vivo Efficacy. *Adv. Ther* **2008**, *25* (10), 979−994.

(18) Das, N.; Madhavan, J.; Selvi, A.; Das, D. An Overview of Cephalosporin Antibiotics as Emerging Contaminants: A Serious Environmental Concern. *3 Biotech* **2019**, *9* (6), 231.

(19) Sullivan, G. J.; Delgado, N. N.; Maharjan, R.; Cain, A. K. How Antibiotics Work Together: Molecular Mechanisms behind Combination Therapy. *Curr. Opin Microbiol* **2020**, *57*, 31−40.

(20) Alitabar-Ferozjah, H.; Rahbar-Kelishami, A. Simultaneous Effect of Multi-Walled Carbon Nanotube and Span85 on the Extraction of Ibuprofen from Aqueous Solution Using Emulsion Liquid Membrane. *J. Mol. Liq.* **2022**, *365*, No. 120051.

(21) Ahmad, N.; Saad, N. Effects of Antibiotics on Dental Implants: A Review. *J. Clin Med. Res.* **2012**, *4* (1), 1−6.

(22) Grenni, P.; Ancona, V.; Barra Caracciolo, A. Ecological Effects of Antibiotics on Natural Ecosystems: A Review. *Microchemical Journal* **2018**, *136*, 25−39.

(23) Couce, A.; Blázquez, J. Side Effects of Antibiotics on Genetic Variability. *FEMS Microbiol Rev.* **2009**, *33* (3), 531−538.

(24) Iwu, C. D.; Korsten, L.; Okoh, A. I. The Incidence of Antibiotic Resistance within and beyond the Agricultural Ecosystem: A Concern for Public Health. *Microbiologyopen* **2020**, *9* (9), No. e1035.

(25) Yang, Y.; Song, W.; Lin, H.; Wang, W.; Du, L.; Xing, W. Antibiotics and Antibiotic Resistance Genes in Global Lakes: A Review and Meta-Analysis. *Environ. Int.* **2018**, *116*, 60−73.

(26) Feng, G.; Huang, H.; Chen, Y. Effects of Emerging Pollutants on the Occurrence and Transfer of Antibiotic Resistance Genes: A Review. *J. Hazard Mater.* **2021**, *420*, No. 126602.

(27) Roy, N.; Alex, S. A.; Chandrasekaran, N.; Mukherjee, A.; Kannabiran, K. A Comprehensive Update on Antibiotics as an Emerging Water Pollutant and Their Removal Using Nano-Structured Photocatalysts. *Journal of Environmental Chemical Engineering* **2021**, *9* (2), No. 104796.

(28) Wei, Z.; Liu, J.; Shangguan, W. A Review on Photocatalysis in Antibiotic Wastewater: Pollutant Degradation and Hydrogen Production. *Chinese Journal of Catalysis* **2020**, *41* (10), 1440−1450.

(29) Naeinimohammadi, S.; Rahbar-Kelishami, A. Fabrication of Nanourchin-like of Iron-Manganese Oxide Composite for the Removal

of Diclofenac Sodium from Aqueous Solution. *Surfaces and Interfaces* **2023**, *36*, No. 102614.
(30) Shayesteh, H.; Nodehi, R.; Rahbar-Kelishami, A. Trimethylamine Functionalized Clay for Highly Efficient Removal of Diclofenac from Contaminated Water: Experiments and Theoretical Calculations. *Surfaces and Interfaces* **2020**, *20*, No. 100615.
(31) Ben, W.; Qiang, Z.; Pan, X.; Chen, M. Removal of Veterinary Antibiotics from Sequencing Batch Reactor (SBR) Pretreated Swine Wastewater by Fenton's Reagent. *Water Res.* **2009**, *43* (17), 4392−4402.
(32) Chamberlain, E.; Adams, C. Oxidation of Sulfonamides, Macrolides, and Carbadox with Free Chlorine and Monochloramine. *Water Res.* **2006**, *40* (13), 2517−2526.
(33) Hu, L.; Martin, H. M.; Strathmann, T. J. Oxidation Kinetics of Antibiotics during Water Treatment with Potassium Permanganate. *Environ. Sci. Technol.* **2010**, *44* (16), 6416−6422.
(34) Salahi, S.; Parvini, M.; Ghorbani, M. Equilibrium Studies in Adsorption of Hg(II) from Aqueous Solutions Using Biocompatible Polymeric Polypyrrole-Chitosan Nanocomposite. *Polycyclic Aromatic Compounds* **2014**, *34* (3), 225−236.
(35) Sadia, M.; Ahmad, I.; Ali, F.; Zahoor, M.; Ullah, R.; Khan, F. A.; Ali, E. A.; Sohail, A. Selective Removal of the Emerging Dye Basic Blue 3 via Molecularly Imprinting Technique. *Molecules* **2022**, *27* (10), 3276.
(36) Ji, L.; Chen, W.; Duan, L.; Zhu, D. Mechanisms for Strong Adsorption of Tetracycline to Carbon Nanotubes: A Comparative Study Using Activated Carbon and Graphite as Adsorbents. *Environ. Sci. Technol.* **2009**, *43* (7), 2322−2327.
(37) Ocampo-Pérez, R.; Rivera-Utrilla, J.; Gómez-Pacheco, C.; Sánchez-Polo, M.; López-Peñalver, J. J. Kinetic Study of Tetracycline Adsorption on Sludge-Derived Adsorbents in Aqueous Phase. *Chemical Engineering Journal* **2012**, *213*, 88−96.
(38) Ahmed, M. B.; Zhou, J. L.; Ngo, H. H.; Guo, W. Adsorptive Removal of Antibiotics from Water and Wastewater: Progress and Challenges. *Science of The Total Environment* **2015**, *532*, 112−126.
(39) Fakhri, A.; Behrouz, S. Comparison Studies of Adsorption Properties of MgO Nanoparticles and ZnO−MgO Nanocomposites for Linezolid Antibiotic Removal from Aqueous Solution Using Response Surface Methodology. *Process Safety and Environmental Protection* **2015**, *94*, 37−43.
(40) Zhao, H.; Liu, X.; Cao, Z.; Zhan, Y.; Shi, X.; Yang, Y.; Zhou, J.; Xu, J. Adsorption Behavior and Mechanism of Chloramphenicols, Sulfonamides, and Non-Antibiotic Pharmaceuticals on Multi-Walled Carbon Nanotubes. *J. Hazard Mater.* **2016**, *310*, 235−245.
(41) Colombo, M.; Carregal-Romero, S.; Casula, M. F.; Gutiérrez, L.; Morales, M. P.; Böhm, I. B.; Heverhagen, J. T.; Prosperi, D.; Parak, W. J. Biological Applications of Magnetic Nanoparticles. *Chem. Soc. Rev.* **2012**, *41* (11), 4306−4334.
(42) Farahmandjou, M.; Honarbakhsh, S.; Behrouzinia, S. PVP-Assisted Synthesis of Cobalt Ferrite (CoFe2O4) Nanorods. *Phys. Chem. Res.* **2016**, *4* (4), 655−662.
(43) Wang, L.; Zhao, H.; Zhang, D.; Song, W.; Xu, S.; Liu, S.; Li, Z. Ordered Mesoporous Carbon-Supported CoFe2O4 Composite with Enhanced Lithium Storage Properties. *J. Mater. Sci.* **2017**, *52* (11), 6265−6279.
(44) Ho, A. Y. Linear and Nonlinear Wave-Particle Interactions. Ph.D. Thesis. Polytechnic Univ.: Brooklyn, NY (United States), 1994, https://www.osti.gov/biblio/135427.
(45) Bashir, B.; Rahman, A.; Sabeeh, H.; Khan, M. A.; Aly Aboud, M. F.; Warsi, M. F.; Shakir, I.; Agboola, P. O.; Shahid, M. Copper Substituted Nickel Ferrite Nanoparticles Anchored onto the Graphene Sheets as Electrode Materials for Supercapacitors Fabrication. *Ceram. Int.* **2019**, *45* (6), 6759−6766.
(46) Kumari, M.; Pittman, C. U.; Mohan, D. Heavy Metals [Chromium (VI) and Lead (II)] Removal from Water Using Mesoporous Magnetite (Fe3O4) Nanospheres. *J. Colloid Interface Sci.* **2015**, *442*, 120−132.
(47) Sani, S.; Adnan, R.; Oh, W.-D.; Iqbal, A. Comparison of the Surface Properties of Hydrothermally Synthesised Fe3O4@C Nanocomposites at Variable Reaction Times. *Nanomaterials* **2021**, *11* (10), 2742.
(48) Ghaedi, M.; Ansari, A.; Sahraei, R. ZnS:Cu Nanoparticles Loaded on Activated Carbon as Novel Adsorbent for Kinetic, Thermodynamic and Isotherm Studies of Reactive Orange 12 and Direct Yellow 12 Adsorption. *Spectrochimica Acta Part A: Molecular and Biomolecular Spectroscopy* **2013**, *114*, 687−694.
(49) Ciabanu, A. A.; Bulgariu, D.; Ionescu, I. A.; Puiu, D. M.; Vasile, G. G.; Bulgariu, L. Evaluation of Thermodynamic Parameters for Cu(II) Ions Biosorption on Algae Biomass and Derived Biochars. *Symmetry* **2023**, *15*, 1500 DOI: 10.3390/sym15081500.
(50) Wang, L.; Chen, G.; Ling, C.; Zhang, J.; Szerlag, K. Adsorption of Ciprofloxacin on to Bamboo Charcoal: Effects of pH, Salinity, Cations, and Phosphate. *Environmental Progress & Sustainable Energy* **2017**, *36* (4), 1108−1115.
(51) Saxena, M.; Sharma, N.; Saxena, R. Highly Efficient and Rapid Removal of a Toxic Dye: Adsorption Kinetics, Isotherm, and Mechanism Studies on Functionalized Multiwalled Carbon Nanotubes. *Surfaces and Interfaces* **2020**, *21*, No. 100639.
(52) Negarestani, M.; Farimaniraad, H.; Mollahosseini, A.; Kheradmand, A.; Shayesteh, H. Facile Preparation of Sisal-Fe/Zn Layered Double Hydroxide Bio-Nanocomposites for the Efficient Removal of Rifampin from Aqueous Solution: Kinetic, Equilibrium, and Thermodynamic Studies. *Int. J. Phytoremediation* **2023**, *25* (5), 586−597.
(53) Langmuir, I. THE ADSORPTION OF GASES ON PLANE SURFACES OF GLASS, MICA AND PLATINUM. *J. Am. Chem. Soc.* **1918**, *40* (9), 1361−1403.
(54) Munagapati, V. S.; Kim, D.-S. Equilibrium Isotherms, Kinetics, and Thermodynamics Studies for Congo Red Adsorption Using Calcium Alginate Beads Impregnated with Nano-Goethite. *Ecotoxicol Environ. Saf* **2017**, *141*, 226−234.
(55) Ortiz-Oliveros, H. B.; Ouerfelli, N.; Cruz-Gonzalez, D.; Avila-Pérez, P.; Bulgariu, L.; Flaifel, M. H.; Abouzeid, F. M. Modeling of the relationship between the thermodynamic parameters ΔH° and ΔS° with temperature in the removal of Pb ions in aqueous medium: Case study. *Chem. Phys. Lett.* **2023**, No. 140329, DOI: 10.1016/j.cplett.2023.140329.
(56) Tang, Y.; Chen, Q.; Li, W.; Xie, X.; Zhang, W.; Zhang, X.; Chai, H.; Huang, Y. Engineering Magnetic N-Doped Porous Carbon with Super-High Ciprofloxacin Adsorption Capacity and Wide pH Adaptability. *Journal of Hazardous Materials* **2020**, *388*, No. 122059.
(57) Kumari, S.; Khan, A. A.; Chowdhury, A.; Bhakta, A. K.; Mekhalif, Z.; Hussain, S. Efficient and Highly Selective Adsorption of Cationic Dyes and Removal of Ciprofloxacin Antibiotic by Surface Modified Nickel Sulfide Nanomaterials: Kinetics, Isotherm and Adsorption Mechanism. *Colloids Surf., A* **2020**, *586*, No. 124264.
(58) Soares, S. F.; Rocha, M. J.; Ferro, M.; Amorim, C. O.; Amaral, J. S.; Trindade, T.; Daniel-da-Silva, A. L. Magnetic Nanosorbents with Siliceous Hybrid Shells of Alginic Acid and Carrageenan for Removal of Ciprofloxacin. *Int. J. Biol. Macromol.* **2019**, *139*, 827−841.
(59) Wang, F.; Yang, B.; Wang, H.; Song, Q.; Tan, F.; Cao, Y. Removal of Ciprofloxacin from Aqueous Solution by a Magnetic Chitosan Grafted Graphene Oxide Composite. *J. Mol. Liq.* **2016**, *222*, 188−194.
(60) Rasoulzadeh, H.; Mohseni-Bandpei, A.; Hosseini, M.; Safari, M. Mechanistic Investigation of Ciprofloxacin Recovery by Magnetite−Imprinted Chitosan Nanocomposite: Isotherm, Kinetic, Thermodynamic and Reusability Studies. *Int. J. Biol. Macromol.* **2019**, *133*, 712−721.
(61) Zhao, P.; Yu, F.; Wang, R.; Ma, Y.; Wu, Y. Sodium Alginate/Graphene Oxide Hydrogel Beads as Permeable Reactive Barrier Material for the Remediation of Ciprofloxacin-Contaminated Groundwater. *Chemosphere* **2018**, *200*, 612−620.
(62) Mao, H.; Wang, S.; Lin, J.-Y.; Wang, Z.; Ren, J. Modification of a Magnetic Carbon Composite for Ciprofloxacin Adsorption. *Journal of Environmental Sciences* **2016**, *49*, 179−188.
(63) Olawale, M. D.; Tella, A. C.; Obaleye, J. A.; Olatunji, J. S. Synthesis, Characterization and Crystal Structure of a Copper-Glutamate Metal Organic Framework (MOF) and Its Adsorptive

https://doi.org/10.1021/acsomega.3c08161
ACS Omega 2024, 9, 6815−6827

Removal of Ciprofloxacin Drug from Aqueous Solution. *New J. Chem.* **2020**, *44* (10), 3961−3969.
(64) Arya, V.; Philip, L. Adsorption of Pharmaceuticals in Water Using Fe3O4 Coated Polymer Clay Composite. *Microporous Mesoporous Mater.* **2016**, *232*, 273−280.
(65) de Franco, M. A. E.; de Carvalho, C. B.; Bonetto, M. M.; Soares, R. de P.; Féris, L. A. Removal of Amoxicillin from Water by Adsorption onto Activated Carbon in Batch Process and Fixed Bed Column: Kinetics, Isotherms, Experimental Design and Breakthrough Curves Modelling. *Journal of Cleaner Production* **2017**, *161*, 947−956.
(66) Mohammadi, A.; Kazemipour, M.; Ranjbar, H.; Walker, R. B.; Ansari, M. Amoxicillin Removal from Aqueous Media Using Multi-Walled Carbon Nanotubes. *Fullerenes, Nanotubes and Carbon Nanostructures* **2015**, *23* (2), 165−169.
(67) Kerkez-Kuyumcu, Ö.; Bayazit, Ş. S.; Salam, M. A. Antibiotic Amoxicillin Removal from Aqueous Solution Using Magnetically Modified Graphene Nanoplatelets. *Journal of Industrial and Engineering Chemistry* **2016**, *36*, 198−205.
(68) Balarak, D.; Joghatayi, A.; Mostafapour, F.; Azarpira, H. Biosorption of Amoxicillin from Contaminated Water onto palm bark Biomass. *Int. J. Life Sci. Pharma. Res.* **2017**, *7*, L-9.
(69) Boukhelkhal, A.; Benkortbi, O.; Hamadache, M.; Ghalem, N.; Hanini, S.; Amrane, A. Adsorptive Removal of Amoxicillin from Wastewater Using Wheat Grains: Equilibrium, Kinetic, Thermodynamic Studies and Mass Transfer. *Desalination and Water Treatment* **2016**, *57* (56), 27035−27047.
(70) Bouyarmane, H.; El Hanbali, I.; El Karbane, M.; Rami, A.; Saoiabi, A.; Saoiabi, S.; Masse, S.; Coradin, T.; Laghzizil, A. Parameters Influencing Ciprofloxacin, Ofloxacin, Amoxicillin and Sulfamethoxazole Retention by Natural and Converted Calcium Phosphates. *J. Hazard Mater.* **2015**, *291*, 38−44.

https://doi.org/10.1021/acsomega.3c08161
ACS Omega 2024, 9, 6815−6827